

# Quantum-hydrodynamic modal perspective on plasmonic gap structures

Pu Zhang ,<sup>\*,†</sup> Christos Tserkezis ,<sup>\*,‡</sup> and N. Asger Mortensen <sup>\*,‡,¶</sup>

<sup>†</sup>*School of physics, Huazhong University of Science and Technology, Luoyu Road 1037, Wuhan 430074, China*

<sup>‡</sup>*POLIMA—Center for Polariton-driven Light–Matter Interactions, University of Southern Denmark, Campusvej 55, DK-5230 Odense M, Denmark*

<sup>¶</sup>*Danish Institute for Advanced Study, University of Southern Denmark, Campusvej 55, DK-5230 Odense M, Denmark*

E-mail: puzhang0702@hust.edu.cn; ct@mci.sdu.dk; asger@mailaps.org

## Abstract

Plasmonic gap structures are among the few configurations capable of generating extreme light confinement, finding applications in surface-enhanced spectroscopy, ultrasensitive detection, photocatalysis and more. Their plasmonic response undergoes a dramatic, quantum effect-driven transition as the gap size approaches zero. Modal analysis can reveal insights into the mechanisms governing this process, which are otherwise obscured by nonlocal damping effects. Here, we offer a fresh modal perspective on the transition of the plasmonic response using quantum hydrodynamic theory (QHT)-based quasinormal mode (QNM) analysis. Focusing on the bonding dipolar and charge-transfer plasmons of a nanosphere dimer, we examine the detailed mode transition through the touching regime as well as the asymptotic behavior compared with the classical results as the constituent nanoparticles either separate or overlap. The complex eigenfrequency particularly provides accurate information on the linewidth and

quality factor of the plasmon modes. We introduce an index to characterize charge-transfer efficiency, especially for the charge-transfer plasmon. The significant role of nonlocal damping in the mode evolution is elucidated by our mode-resolved QHT-QNM analysis. The insights from our theoretical study provide an integrated understanding of mode evolution in plasmonic gap structures, which can further advance gap structure-based applications.

## Introduction

Surface plasmons are collective oscillations of free electrons in a conducting material driven by an optical field. The surface wave behavior tightly localizes the optical field at the interface, bringing about profound physical effects in light confinement and optical processes.<sup>1-3</sup> The nanoscale confinement breaks the diffraction limit,<sup>4</sup> while the enhanced optical field significantly boosts a myriad of light-matter interactions.<sup>2,5-7</sup> The modification of the local density of electromagnetic states by surface plasmons can alter photon emission processes,<sup>8,9</sup> while energetic hot electrons generated through these interactions actively participate in chemical reactions.<sup>10-12</sup> The rich physics enabled by light confinement forms the cornerstone of plasmonics research. In pursuit of stronger confinement, nanostructured metals are highly effective. Metallic nanoparticles (NPs) provide three-dimensional (3D) confinement through resonant localized surface plasmons (LSPs).<sup>13</sup> Sharp tips may concentrate the optical field through a non-resonant lightning-rod effect.<sup>14</sup> Plasmonic gap structures achieve the highest degree of confinement due to both geometric compression and resonant effects.<sup>15</sup> Leveraging plasmonic gap structures enables the study of the aforementioned intriguing physical effects, spawning far-reaching applications such as subwavelength optical microscopy,<sup>4</sup> single-molecule detection through surface-enhanced Raman spectroscopy,<sup>16</sup> bright photon sources due to plasmonic enhancement,<sup>17</sup> and plasmonic photocatalysis,<sup>18</sup> to name a few.

Rapid advances in nanofabrication and nanoscale manipulation techniques have enabled the experimental realization of plasmonic gap structures with increasingly smaller gap sizes

and finely controlled morphologies.<sup>19–22</sup> This aligns with the pursuit of achieving tighter light confinement and enhanced device performance through increased plasmonic effects. Single-digit-nanometer and subnanometer plasmonic gap structures not only provide further qualitative enhancements but also raise important questions about the ultimate limits of plasmonic structures.<sup>23–27</sup> The latter has sparked intense explorations of optical processes with record-breaking plasmonic enhancement factors. For instance, subnanometer resolution has been demonstrated with tip-enhanced spectroscopy,<sup>28,29</sup> where the mode volume of the localized optical field enters the sub-1 nm<sup>3</sup> regime,<sup>30–32</sup> and an average field enhancement of around 10<sup>3</sup> is corroborated.<sup>33</sup> As the gap size approaches the characteristic length scale of electron screening, quantum-related phenomena emerge, potentially expanding or in some cases limiting the application scenarios of plasmonics.<sup>34,35</sup> Inelastic electron tunneling enables electrically-driven plasmon sources,<sup>36,37</sup> strong electron–photon coupling facilitates ultrafast electro-optic modulation,<sup>38,39</sup> and quantum tunneling can trigger nonlinear optical processes.<sup>40</sup> In this regard, the exploitation of nearly-touching gap structures for innovations requires an in-depth understanding of how the plasmonic response evolves as the gap size approaches zero.

To investigate the transition of the response of plasmonic gap structures as the gap size decreases, a theoretical approach is indispensable. Mode hybridization is a conceptually illuminating and sometimes fully adequate analytical theory for analyzing composite plasmonic structures.<sup>41</sup> For example, the plasmonic resonances of a nanoparticle dimer result from the hybridization of the plasmons of its constituent NPs. In order of increasing frequency, we have the bonding-dipolar plasmon (BDP), bonding-quadrupolar plasmon (BQP), and higher-order plasmon modes.<sup>23</sup> When the nanoparticles overlap, the charge-transfer plasmon (CTP) emerges.<sup>42</sup> While the evolution of plasmonic resonances in well-separated dimers is well understood through the hybridization model and classical computational electrodynamics, the situation becomes more complex at nanoscale gap sizes. Non-classical effects, including non-locality, electron spillover, and nonlocal damping, emerge, as evidenced by both experimental

and computational studies.<sup>34,43–47</sup> However, the existing understanding originates almost exclusively from a spectroscopic perspective. As a result, in the transition regime, information about the linewidth, quality factor, and even resonance position of the plasmons cannot be obtained without ambiguity, particularly due to nonlocal damping.<sup>48</sup> Resolving this intricate issue requires a rigorous mode theory that can simultaneously account for non-classical effects.

In this work, we conduct a systematic modal analysis of a plasmonic nanosphere dimer using a quantum hydrodynamic-based quasinormal mode (QNM) theory. We rigorously trace the entire evolution of the dominant plasmon modes, bridging the well-separated and overlapping limits, and identifying critical gap sizes. The analysis accurately reveals how key modal properties, such as the complex eigenfrequency and quality factor, respond to the narrowing gap. For the CTP, we introduce an index to characterize the efficiency of charge transfer across the gap. Moreover, the modal analysis enables a quantitative assessment of the significance of nonlocal damping in a mode-resolved manner.

## Methodology

Before delving into the results, we elaborate on the theoretical method necessary for systematically studying plasmonic gap structures with gap sizes ranging from positive to negative values. Considering the relevant deca-nanometer particle size and the need for compatibility with QNM theory, we must adopt a semiclassical approach rather than relying on first-principles methods. Among the popular semiclassical models,<sup>49–52</sup> self-consistent QHT stands out for its ability to describe all relevant non-classical effects, particularly the detailed stationary electron distribution in the gap region.<sup>53–57</sup> Regarding the QNM theory,<sup>58,59</sup> several extensions have been developed beyond the classical formulation.<sup>60–63</sup> In particular, one of us recently reported the generalized Lorentz model (GLM),<sup>61</sup> which enables the establishment of a QNM theory based on any continuum response models, including QHT. Therefore,

we deploy QHT and the corresponding QNM theory in this work.

In QHT, the conduction electrons responsible for the plasmonic response of a metallic structure are characterized by the electron density  $n(\mathbf{r}, t)$  and the velocity field  $\mathbf{v}(\mathbf{r}, t)$ . Restricting to the linear response under weak light excitation, the plasmon is built perturbatively on the stationary distribution  $n_0(\mathbf{r})$ . Here,  $n_0(\mathbf{r})$  is self-consistently determined by solving the force equilibrium equation

$$\nabla \left( \frac{\delta G}{\delta n} \right)_0 - q_e \mathbf{E}_0 = 0 \quad (1)$$

together with Poisson's equation  $\nabla^2 \phi_0 = (n_+ - n_0)q_e/\varepsilon_0$ . The subscript "0" denotes the stationary components. The electrostatic field is related with the static potential as  $\mathbf{E}_0 = -\nabla \phi_0$ . In eq 1, the non-classical force derives from the internal energy functional  $G = \int d\mathbf{r} g[n(\mathbf{r}, t)]$ . The energy density  $g[n(\mathbf{r}, t)] = t_{\text{TF}} + t_{\text{W}} + e_{\text{XC}}$  consists of the Thomas–Fermi kinetic energy  $t_{\text{TF}} = \frac{\hbar^2 \pi^3}{10m_e} \left( \frac{3n}{\pi} \right)^{5/3}$ , the von Weizsäcker kinetic energy  $t_{\text{W}} = \frac{\lambda_{\text{W}} \hbar^2}{8m_e} \frac{\nabla n \cdot \nabla n}{n}$ , and the exchange-correlation energy  $e_{\text{XC}} = - \left( 0.0588 + \frac{0.035}{0.6204 + 7.8 \times a_{\text{H}} n^{1/3}} \right) \frac{q_e^2}{\varepsilon_0} n^{4/3}$ . In the above,  $\varepsilon_0$ ,  $\hbar$ ,  $a_{\text{H}} = 0.529 \text{ \AA}$ ,  $q_e < 0$ ,  $m_e$ ,  $\lambda_{\text{W}} = 0.12$ , and  $n_+$  denote respectively the vacuum permittivity, the reduced Planck constant, the Bohr radius, the electron charge, the electron mass, the von Weizsäcker parameter, and the uniform number density for the positive ionic lattice according to the jellium approximation. For the exchange-correlation energy, Wigner's local-density approximation is employed. The  $n_0$  distribution, incorporating the above non-classical contributions, can accurately describe electron spillover both at the surface and in the gap region.

On top of the stationary electron distribution, the linear plasmonic response follows from

$$(-i\omega + \gamma)\mathbf{J} = \frac{q_e}{m_e} \left[ n_0 q_e \mathbf{E} - n_0 \nabla \left( \frac{\delta G}{\delta n} \right)_1 + \nabla \cdot \bar{\sigma} \right] \quad (2)$$

in terms of the induced electron density  $n_1(\mathbf{r}, t)$  and the current density  $\mathbf{J}(\mathbf{r}, t) = n_0(\mathbf{r})q_e \mathbf{v}(\mathbf{r}, t)$ .

The linear-order terms are indexed with a subscript "1" in cases of ambiguity, and we have

already suppressed the factor  $e^{-i\omega t}$  according to the assumed time-harmonic convention. Here, the non-classical effects manifest themselves in the plasmonic response through the linear-order components of  $\frac{\delta G}{\delta n}$ . Apart from the phenomenological damping with the rate of  $\gamma$ , a non-adiabatic energy functional in QHT serves as an effective avenue to model the nonlocal damping. A current-dependent functional proves to be sufficiently effective for the current purpose and appears as the viscous stress tensor  $\bar{\sigma}$  in eq 2.<sup>56</sup> The Cartesian components of  $\bar{\sigma}$  are given by  $\sigma_{\mu\nu} = \eta_k(\frac{\partial v_\mu}{\partial x_\nu} + \frac{\partial v_\nu}{\partial x_\mu} - \frac{2}{3}\delta_{\mu\nu}\nabla \cdot \mathbf{v})$  with the coefficient  $\eta_k = 14\hbar \left(60r_{s0}^{-3/2} + 80r_{s0}^{-1} - 40r_{s0}^{-2/3} + 62r_{s0}^{-1/3}\right)^{-1} n_0$  and the position-dependent Wigner–Seitz radius  $r_{s0} = \sqrt[3]{3/(4\pi a_H^3 n_0)}$ . By coupling with Maxwell’s equations and the continuity equation,  $-i\omega q_e n_1 + \nabla \cdot \mathbf{J} = 0$ , eq 2 forms the closed linear-response theory. In studying the transition of the plasmonic response, the inhomogeneous  $n_0$  distribution and nonlocal damping play a significant role. To underscore their impact, we also compare with a hydrodynamic theory (HT) that assumes a homogeneous  $n_0 = n_+$  and neglects nonlocal damping. The linear response according to this HT is typically governed by<sup>52,64</sup>

$$\beta^2 \nabla(\nabla \cdot \mathbf{J}) + \omega(\omega + i\gamma)\mathbf{J} = i\omega\omega_p^2 \varepsilon_0 \mathbf{E}. \quad (3)$$

Here,  $\omega_p^2 = q_e^2 n_+ / (m_e \varepsilon_0)$  is the plasma frequency. The parameter  $\beta$  can be understood as a characteristic velocity, arising from the Thomas–Fermi energy.<sup>65,66</sup> As an energy functional of  $n_0$ , the local-density approximation of exchange–correlation similarly contributes to this parameter. For the Wigner exchange–correlation approximation and the metal sodium (Na) concerned in this work, we find the parameter takes the value  $\beta = \sqrt{12/125}v_F$ .

In addition to the direct calculation of the linear response, a QHT-based QNM theory is required to conduct modal analysis. As a continuum theory, QHT fits into the GLM. For the linear response, eq 2 can be reformulated as<sup>61</sup>

$$\omega^2 \mathbf{P} + i\omega\rho\hat{\Gamma}\mathbf{P} - \rho\hat{\Theta}\mathbf{P} + \varepsilon_0\omega_p^2\rho\mathbf{E} = 0, \quad (4)$$

where  $\mathbf{P}$  and  $\rho = n_0/n_+$  are the polarization field and the normalized stationary electron density, respectively. The nonlocal damping and restoring force operators of the QHT turn out to be

$$[\hat{\Gamma}_1]_{jj'} = \frac{2}{3} \frac{\delta_{ij}\delta_{i'j'} - \delta_{i'j}\delta_{ij'} - \delta_{i'i}\delta_{jj'}}{m_e n_+} \frac{\partial_i}{\rho} \left[ \eta_k \partial_{i'} \left( \frac{1}{\rho} \cdot \right) \right], \quad (5a)$$

$$\hat{\Theta} = \nabla K_1(\nabla \cdot) - \nabla \nabla \cdot K_2 \nabla(\nabla \cdot), \quad (5b)$$

where  $K_1$  and  $K_2$  are both functions of  $\rho$ .<sup>61</sup> The full damping-force operator is given by  $\hat{\Gamma} = \hat{\Gamma}_1 + \gamma/\rho$ . Written in the GLM form, eq 2 conveniently converts into a linear eigenvalue problem with the eigenvalue  $\omega$  and eigenvector  $[\mathbf{E}, \mathbf{H}, \mathbf{P}, \mathbf{J}]$ . The latter defines the QNM in QHT. More importantly, the GLM formulation also provides a framework upon which the theorems for local-response electromagnetic media can be generalized to non-classical ones. From the generalized Poynting theorem, we identify the absorption power to be

$$\mathbf{P}_{\text{abs}} = \frac{1}{\varepsilon_0 \omega_p^2} \int_{\Omega} d\mathbf{r} \mathbf{J} \cdot \left( \hat{\Gamma}_1^* + \frac{\gamma}{\rho} \right) \mathbf{J}^*. \quad (6)$$

The absorption consists of two components:  $\mathbf{P}_{\text{abs,NL}}$  due to nonlocal damping and the phenomenological part  $\mathbf{P}_{\text{abs},0}$ . The HT, as a simplified version of the QHT, is essentially a specialized form of the GLM, with the force operators given by  $\hat{\Theta} = -\nabla \beta^2(\nabla \cdot)$  and  $\hat{\Gamma} = \gamma$ . The QNM theory for HT then follows from the GLM framework.

## Results and discussion

Prevalent in plasmonics, a nanogap can be constructed in various plasmonic structures, including, *e.g.*, nanoparticle dimers,<sup>67</sup> particle assemblies,<sup>68</sup> and particle-on-mirror configurations.<sup>3</sup> Without loss of generality, in this work we use a nanosphere dimer as an example of typical plasmonic gap structures. As sketched in the insets of Figure 1, the dimer consists of two sodium nanospheres of diameter  $D = 20$  nm, with the gap size  $g$  varying from positive to negative, the latter corresponding to overlapping spheres. The material is assumed to be the

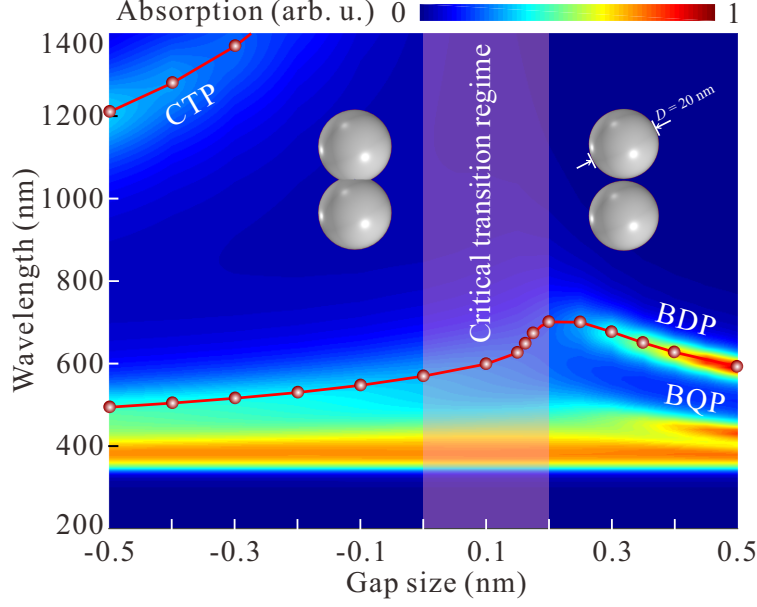


Figure 1: Colormap of the absorption spectrum as a function of wavelength  $\lambda$  and gap size  $g$  for an incident plane wave polarized along the axis of a  $D = 20$  nm sodium nanosphere dimer (see insets). The bonding dipolar plasmon (BDP) and charge-transfer plasmon (CTP) modes are traced (red lines), and superimposed on those data points obtained from QNM analysis.

simple alkali metal sodium (Na) in order to relieve our study from the influence of the bound electrons typically contributing to the optical response of noble metals. Sodium has a bulk electron density  $n_+ = 2.52 \times 10^{28} \text{ m}^{-3}$  and phenomenological damping rate  $\gamma = 0.066 \text{ eV}$ . To set the stage for the discussion, we first examine the plasmonic response of the dimer from the spectroscopic perspective. We assume a plane wave polarized along the dimer axis incident on the dimer to excite the LSP modes of interest. Solving eq 2, we obtain the absorption spectra of the dimer for  $g \in [-0.5, 0.5] \text{ nm}$ , as rendered into the colormap in Figure 1. We designate the shaded gap size region with  $g \in [0, 0.2] \text{ nm}$  as the critical transition regime (CTR). When  $g > 0.2 \text{ nm}$ , the plasmons of the individual NPs are capacitively coupled, with the coupling strength increasing as the gap size decreases. Due to strong hybridization, both the BDP and BQP redshift, moving out of the major resonance formed by the coalescing higher-order plasmons. For the overlapped dimer, while the CTP beyond  $1 \mu\text{m}$  is clearly observable, another plasmon manifests vaguely as a shoulder around the  $500 \text{ nm}$



wavelength range. The identity of this latter plasmon cannot be easily discerned from the spectrum, and it is sometimes assigned as the second charge-transfer plasmon (CTP') in the literature.<sup>69,70</sup> The difficulty arises partly due to the significantly broadened and merged resonance caused by nonlocal damping. In the CTR, nonlocal damping, along with electron spillover, can make the spectra nearly featureless. As a result, it is intricate to unravel how the plasmonic resonance properties of the dimer are correlated between the separated and overlapped regimes. We focus on the fundamental CTP and BDP, and superimpose their eigenwavelengths (real parts) onto the colormap in Figure 1. Outside the CTR, the eigenwavelength data from the QNM theory clearly overlap with the resonance peak or shoulder positions in the spectra. Inside the CTR, the eigenwavelength data unequivocally disclose that the BDP continuously evolves across the CTR. With the superimposed data points, the imaginary parts of the eigenwavelengths are discarded. A complete picture is obtained when the full information from the QNMs is considered.

We begin the QNM analysis with the BDP, which typically contributes the strongest plasmonic enhancement. Applying the QHT-based QNM theory, we find the BDP mode of the dimer across an extended range of gap sizes,  $g \in [-5, 5]$  nm. The evolution of the BDP mode is visualized on the complex frequency plane in Figure 2a, with the gap size indicated by the color of the circle markers. Note that tracing on the complex wavelength plane is another viable option for visualizing the mode evolution. We opt for the present choice because both the real and the imaginary parts of a complex frequency have clear physical meanings, considering the time-harmonic factor  $e^{-i(\omega_R - i|\omega_I|)t}$  used to describe an optical field in the frequency domain. With the gap size spanning both the well-separated and the overlapped cases, the eigenfrequency trace demonstrates the entire evolution. Both the real and imaginary parts exhibit a back-bending feature. The resonance frequency initially redshifts as the capacitive coupling augments with the gap size approaching the CTR from the positive side. Then, as the gap size decreases further, the coupling is diminished by nonlocality and electron spill-out, causing the BDP to blueshift. In contrast, the similar

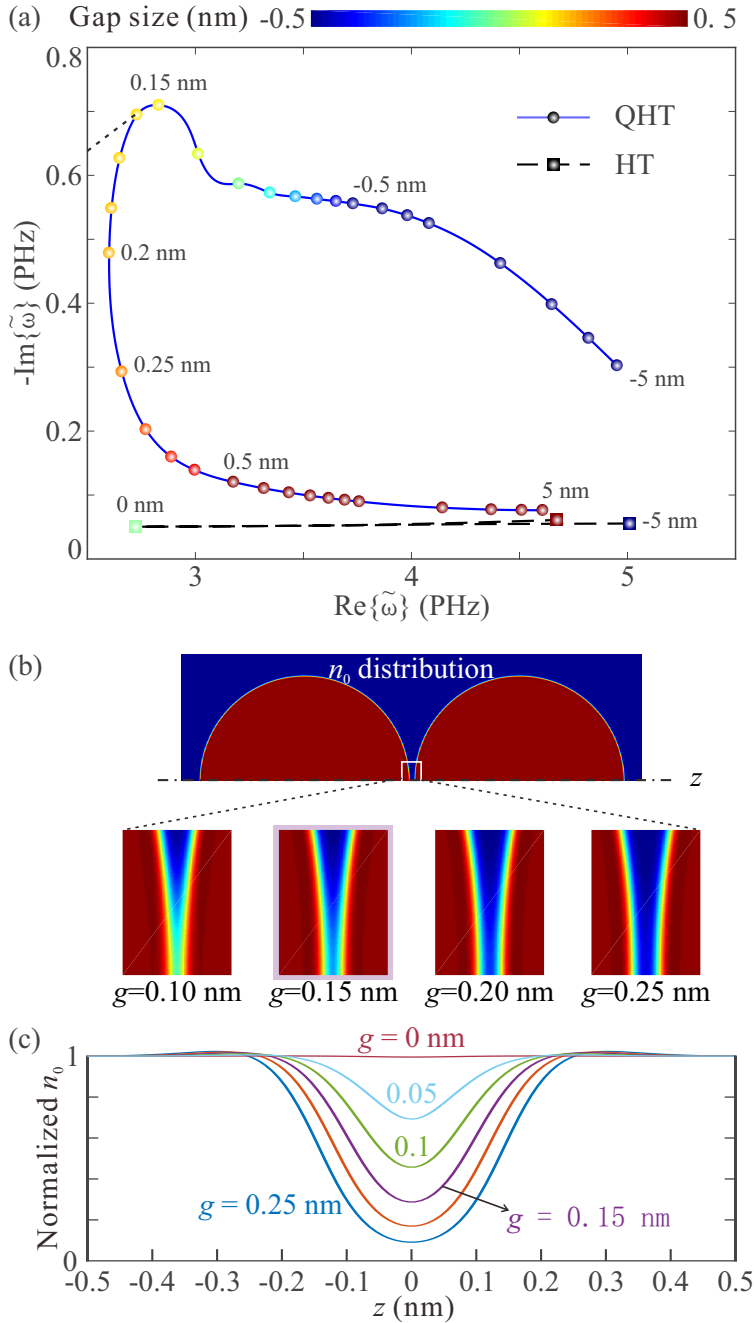


Figure 2: Bonding dipolar plasmon mode evolution. (a) The eigenfrequencies of the BDP mode according to the quantum hydrodynamic (solid lines, circles) and hard-wall hydrodynamic (long dashed lines, squares) theories on the complex frequency plane. The color of the markers denotes the gap size. The thin dashed line on the top-left corner points to the origin of the coordinate and marks the lowest-quality factor region. (b) The stationary electron density  $n_0$  distributions in the gap region when the gap size crosses the threshold for quantum tunneling. (c) The  $n_0$  distributions on the dimer axis for a series of positive gap sizes.

back-bending behavior of the imaginary part results from the maximal nonlocal damping occurring in the CTR. To emphasize the impact of electron spill-out and nonlocal damping, we also present in Figure 2a the eigenfrequency trace of the BDP calculated using HT, indicated by the square markers. The evolution according to HT correctly reflects the rise and fall of the coupling strength as electron nonlocality is considered. However, the much-simplified overall pattern and the nearly constant imaginary part result from the neglect of electron spill-out and nonlocal damping. At large gap sizes, the two methods agree well; however, there is still a sizable discrepancy in the imaginary part even when the gap size is  $g = -5$  nm. The discrepancy arises because nonlocal damping remains significant for the overlapped dimer, as will be discussed later.

Next, we elaborate on the extrema associated with the back-bending pattern. The maximum of the real part occurs at  $g_R = 0.2$  nm, which precisely marks the entry into the CTR. More dramatic transition takes place inside the CTR. The nonlocal damping and hence the imaginary part peak at the gap size of  $g_I = 0.15$  nm. The ordering of the appearance of the extrema lies in the distinct underlying mechanisms. While the capacitive coupling strength falls once non-classical effects start to engage, other important aspects only respond to the electron spill-out effect at a smaller gap. Inside the CTR the field confinement continues growing stronger with the shrinking gap until the electron screening by the spill-out puts an end to the growth. Concomitantly, the maximal nonlocal damping and imaginary part are accompanied by the emergence of a considerable electron spill-out. These arguments are in fact supported by the stationary electron distributions obtained with the self-consistent QHT. As illustrated in Figure 2b, the electron density  $n_0$  in the gap region is negligible for  $g \geq 0.2$  nm, and becomes visible at  $g \leq 0.15$  nm. The  $n_0$  distributions along the dimer axis are further depicted in Figure 2c for a quantitative description. 30% of the homogeneous  $n_+$  appears as the threshold to trigger the extrema. The imaginary part of the eigenfrequency is related to another key property of the BDP plasmon mode, *i.e.* the quality factor  $Q$ . Defined as  $Q = \omega_R/2|\omega_I|$ , it is directly determined by the slope of the line connecting the

origin and a point on the trace. The lowest quality factor obviously occurs at the point where the line directing to the origin coincides with the tangent of the trace. In Figure 2a, the lowest quality factor point is pictorially pinpointed with the dashed tangent line. The corresponding gap size is 0.16 nm, only slightly larger than  $g_I$  which we deem as a more critical gap size during the transition.

The CTP appears as the sole resonance in the long wavelength range as witnessed at the top-left corner of Figure 1. It is of particular interest owing to its sensitivity to the conductance of the nanogap and as a unique resonance extendable to the terahertz range. We proceed to the QNM analysis of the CTP in this section. By employing the QHT based QNM theory, we trace the CTP mode for the gap sizes from  $-5$  nm until it practically ceases to exist. The resulting trace is presented in Figure 3a. Since the CTP is well defined for the overlapped dimer, we embark on the discussion starting from the negative gap sizes. The real part of the eigenfrequency exhibits a monotonous redshift with increasing gap size. The rate of redshifting is, however, remarkably accelerated after entering the positive gap size range. The observation can be interpreted by associating the CTP resonance frequency with the time required to transfer the charge between the NPs and thus with the conductance of the nanogap.<sup>71</sup> During the transition from the overlapped to kissing dimer, the two NPs essentially remain connected with a conducting neck, so that the conductance decreases slowly and the redshift is moderate. After entering the CTR, the conducting neck quickly disappears with the opening of the gap. The conductance drops abruptly, causing the resonance frequency of the CTP to plunge by more than two orders of magnitude. On the other hand, the imaginary part pertinent to dissipation has a maximum in the transition process. This happens because the CTP suffers a maximal nonlocal damping in the CTR as does the BDP. Interestingly, meanwhile the resistance hikes due to the thinning of electron density in the opening gap, the dissipation becomes alleviated for the further separated dimer. Nevertheless, the quality factor of the CTP mode is decreasing all the way as given by the inverse of the slope. In the end, the CTP ceases to exist as the linewidth relative

to the resonance frequency diverges. This is consistent with the fact that the CTP does not have a counterpart for the individual NPs and cannot be properly understood with the hybridization theory. Without the electron spillover, HT cannot provide a full description of the CTP. The HT-based QNM theory only describes the CTP mode for the overlapped dimer, as illustrated in Figure 3a. The redshift of the resonance is predicted with a good accuracy, but the imaginary part again changes little as only the constant phenomenological damping is included in the HT. The nonlocal damping as indicated by the discrepancy with the QHT is yet not as severe as for the BDP.

Charge transfer between the constituent NPs is the most prominent feature of the CTP. However, there still lacks an index to evaluate the performance of the CTP for the task. Moreover, in a general sense, other plasmons like the BDP are also referred to as CTPs, as long as they persist for the overlapped dimer. It is not clear whether these CTPs are as capable as the fundamental CTP of transferring electrons. To this end we propose the charge-transfer ratio defined as below

$$r_{\text{CT}} = \left| \int_{\text{NP1}} \tilde{n}_1 dV \right| / \int_{\text{NP1}} |\tilde{n}_1| dV, \quad (7)$$

where  $\tilde{n}_1$  stands for the induced electron density of the plasmonic eigenmode, and the volume integrals are performed for one nanoparticle (NP1). The ratio is intended to characterize the proportion of the induced electrons displaced from the other nanoparticle (NP2) in the total induced electrons in NP1. Once some local polarization occurs within NP1, the corresponding contribution to  $\tilde{n}_1$  cancels in the numerator but not in the denominator, so that  $r_{\text{CT}}$  becomes smaller than unity. Only when all the induced electrons come from NP2, does  $r_{\text{CT}}$  reach the maximum or unity. As such, the charge-transfer ratio  $r_{\text{CT}}$  assesses the purity of a plasmon as a CTP. We note that this ratio only offers the delineation of one aspect of a CTP. Other aspects like the strength of the oscillation are needed for a complete description. We specifically evaluate  $r_{\text{CT}}$  for the CTP and depict it as a function of the gap

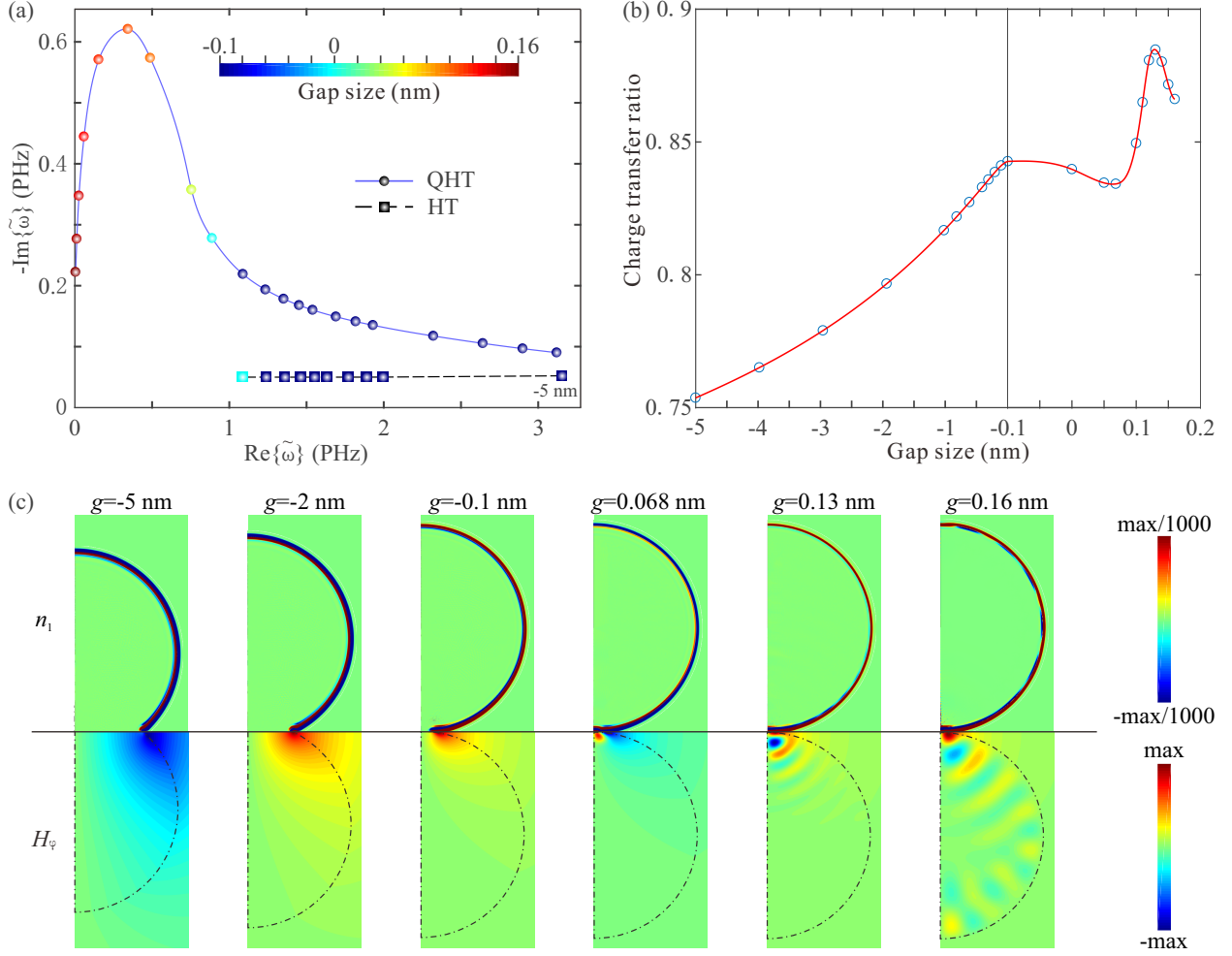


Figure 3: CTP mode evolution. (a) The eigenfrequencies of the CTP mode according to QHT (solid lines) and HT (dashed line) on the complex frequency plane. The color of the markers denotes the gap size. (b) The charge-transfer ratio (defined in eq 7) of the CTP as a function of the gap size. The abscissa from  $-0.1$  nm to  $0.2$  nm is zoomed-in to resolve the variations. (c) The modal distributions of the induced electron density  $\tilde{n}_1$  (upper panels) and magnetic field  $\tilde{H}_\phi$  (lower panels) for the CTPs at a series of representative gap sizes.

size in Figure 3b. The results undoubtedly prove the CTP indeed boasts a pretty high  $r_{CT}$ , generally above 75%. In contrast, we find that the value for the BDP stays below 20% for the overlapped dimer. We focus on the ratio for the CTP, which displays a nontrivial variation with the gap size. The charge-transfer ratio  $r_{CT}$  continuously grows to about 85%, until the gap size closes in on the CTR; then a dip and a peak occur within the CTR. We try to interpret the nontrivial variation with the help of the modal profiles. The induced electron density and magnetic field patterns are showcased respectively in the upper and lower panels of Figure 3c for a series of representative gap sizes. For all the cases,  $n_1$  concentrates near the NP surface. More interestingly, multilayers of alternate signs form along the radial direction, indicating that the CTP assumes a multipole plasmon feature. Such a multipole plasmon feature apparently limits  $r_{CT}$  to a lower value. In fact, the initial rise of  $r_{CT}$  with the gap size is observed to pertain to the gradual weakening of the multipolar pattern. Inside the CTR,  $r_{CT}$  declines slightly upon the breakup of the conducting neck. Afterwards,  $r_{CT}$  goes on to rise and culminates at the 0.13 nm gap, when the multipolar pattern nearly disappears. From this point on, the imaginary part of the eigenfrequency starts to dominate over the real part, and the modal profiles or the responses at the eigenfrequency may differ from the responses to a real-frequency excitation. For instance, the latter two modal magnetic fields in Figure 3c propagate with a much shorter wavelength across the NP, rather than decay monotonously inside the metal as in the former cases. The interference pattern then induces extra polarization at the surface, causing  $r_{CT}$  to decline. We remark, in passing, that  $r_{CT}$  can be calculated for a response to a real-frequency excitation and maintains the high level for the CTP at real frequency.

As we have demonstrated, nonlocal damping plays an essential role in the plasmon evolution. But these observations are based so far on qualitative and comparative analysis. In the last section we take advantage of the GLM formulation of QHT to quantify the contribution of nonlocal damping. To be specific, eq 6 allows to explicitly separate the total absorption

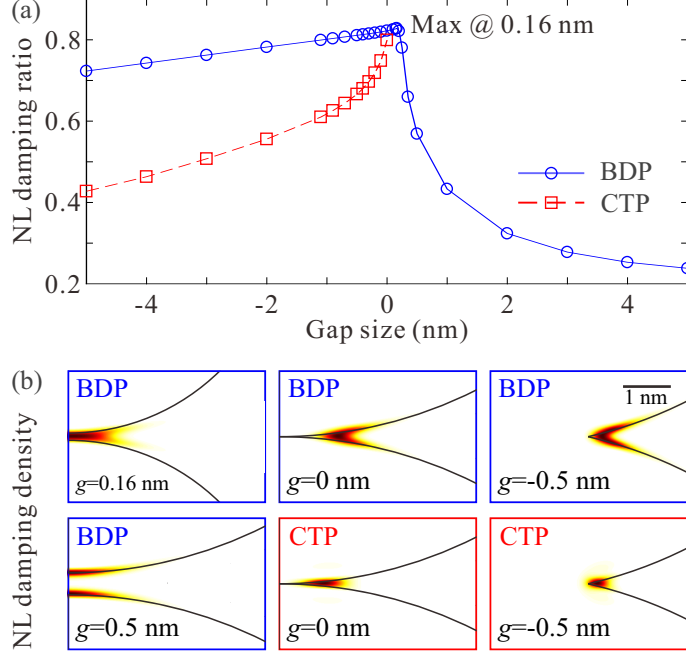


Figure 4: Nonlocal damping contribution to the absorption of the sodium dimer. (a) The nonlocal damping ratio (defined in eq 8) as functions of the gap size for both BDP (blue line, circles) and CTP (red line, squares). (b) The power density of the nonlocal damping in the gap region for the representative cases denoted in the label of each panel.

into nonlocal and phenomenological contributions. We therefore introduce the nonlocal ratio

$$r_{\text{NL}} = P_{\text{abs,NL}}/P_{\text{abs}} \quad (8)$$

to quantitatively characterize the contribution of nonlocal damping. Additionally, the expression of the absorption density facilitates the visualization of the spatial distribution of the nonlocal damping. We compute  $r_{\text{NL}}$  for both the BDP and CTP. Since the dissipation at a complex frequency is not easily defined, the ratio is evaluated at the real part of the eigenfrequencies. We plot the results against the gap size in Figure 4a. As expected, the  $r_{\text{NL}}$  traces maximize with  $r_{\text{NL}} > 80\%$  in the CTR, and decay for both the overlapped and separated dimers. For the BDP, the maximal  $r_{\text{NL}}$  occurs at the same gap size when the quality factor minimizes. The nonlocal damping is strongly enhanced in the gap region, as shown in Figure 4b. Outside the CTR,  $r_{\text{NL}}$  decays much faster at the positive gaps than



for the overlapped dimer. This is consistent with the the nonlocal damping distributions given in Figure 4b. While only feeble nonlocal damping remains at the opposite surfaces of the gap, it is squeezed at the sharp corner of the neck in the overlapped dimer. The ratio is even still above 75% at the -5 nm gap. The sizable nonlocal damping explains the large discrepancy in the imaginary part of the eigenfrequency computed by QHT and HT. In comparison, nonlocal damping decays to about 40% at the  $-5$  nm gap for the CTP. We can tell the difference from the nonlocal damping distributions in Figure 4b. The nonlocal damping density is squeezed into a smaller region in the corner for the CTP than the BDP, resulting in relatively weak damping.

## Conclusion

We analyzed mode-transition processes in plasmonic nanogaps, and explored the roles of electron spill-out and nonlocal damping. Employing a recently developed QNM theory in the QHT framework, we were able to self-consistently follow the evolution of both the real and the imaginary parts of the eigenfrequencies of a sodium nanosphere dimer, shedding light on the distinct mechanisms behind their nontrivial evolution for both the BDP and the main CTP. In particular, the imaginary part quantitatively reveals how the key properties associated with nonlocal damping, including the linewidth and quality factor, evolve in the transition regime. The vanishing quality factor of the CTP mode with the opening gap helps rationalize its gradual disappearance in the separated dimer. We further introduced a charge-transfer index that allows to clearly demonstrate the CTP's prominent efficiency of transporting electrons between the nanoparticles. Lastly we quantified the contributions of different origins to plasmonic damping, unveiling the dominance of nonlocal damping in the nearly touching and overlapped situations. While focused on nanosphere dimers, our conclusions generally apply to any other gap structure, and provide a deeper understanding of the physics governing plasmonic nanogaps of Ångström size.

## Acknowledgement

The Center for Polariton-driven Light–Matter Interactions (POLIMA) is sponsored by the Danish National Research Foundation (Project No. DNRFF165). P. Z. acknowledges financial support from the National Natural Science Foundation of China (Grant No. 12274160).

## References

- (1) Schuller, J. A.; Barnard, E. S.; Cai, W.; Jun, Y. C.; White, J. S.; Brongersma, M. L. Plasmonics for extreme light concentration and manipulation. *Nat. Mater.* **2010**, *9*, 193–204.
- (2) Halas, N. J.; Lal, S.; Chang, W.-S.; Link, S.; Nordlander, P. Plasmons in strongly coupled metallic nanostructures. *Chem. Rev.* **2011**, *111*, 3913–3961.
- (3) Baumberg, J. J.; Aizpurua, J.; Mikkelsen, M. H.; Smith, D. R. Extreme nanophotonics from ultrathin metallic gaps. *Nat. Mater.* **2019**, *18*, 668–678.
- (4) Gramotnev, D. K.; Bozhevolnyi, S. I. Plasmonics beyond the diffraction limit. *Nat. Photon.* **2010**, *4*, 83–91.
- (5) Xu, H.; Aizpurua, J.; Käll, M.; Apell, P. Electromagnetic contributions to single-molecule sensitivity in surface-enhanced Raman scattering. *Phys. Rev. E* **2000**, *62*, 4318–4324.
- (6) Acuna, G. P.; Möller, F. M.; Holzmeister, P.; Beater, S.; Lalkens, B.; Tinnefeld, P. Fluorescence enhancement at docking sites of DNA-directed self-assembled nanoantennas. *Science* **2012**, *338*, 506–510.
- (7) Yu, H.; Peng, Y.; Yang, Y.; Li, Z.-Y. Plasmon-enhanced light-matter interactions and applications. *npj Comp. Mater.* **2019**, *5*, 45.

- (8) Gonçalves, P. A. D.; Christensen, T.; Rivera, N.; Jauho, A.-P.; Mortensen, N. A.; Soljačić, M. Plasmon–emitter interactions at the nanoscale. *Nat. Commun.* **2020**, *11*, 366.
- (9) Zhang, P.; Protsenko, I.; Sandoghdar, V.; Chen, X.-W. A single-emitter gain medium for bright coherent radiation from a plasmonic nanoresonator. *ACS Photonics* **2017**, *4*, 2738–2744.
- (10) Brongersma, M. L.; Halas, N. J.; Nordlander, P. Plasmon-induced hot carrier science and technology. *Nat Nanotechnol.* **2015**, *10*, 25–34.
- (11) Li, W.; Valentine, J. G. Harvesting the loss: surface plasmon-based hot electron photodetection. *Nanophotonics* **2017**, *6*, 177–191.
- (12) Khurgin, J. B. Hot carriers generated by plasmons: where are they generated and where do they go from there? *Faraday Discuss.* **2019**, *214*, 35–58.
- (13) Le, F.; Brandl, D. W.; Urzhumov, Y. A.; Wang, H.; Kundu, J.; Halas, N. J.; Aizpurua, J.; Nordlander, P. Metallic nanoparticle arrays: a common substrate for both surface-enhanced Raman scattering and surface-enhanced infrared absorption. *ACS Nano* **2008**, *2*, 707–718.
- (14) Stockman, M. I. Nanofocusing of optical energy in tapered plasmonic waveguides. *Phys. Rev. Lett.* **2004**, *93*, 137404.
- (15) Kern, J.; Großmann, S.; Tarakina, N. V.; Häckel, T.; Emmerling, M.; Kamp, M.; Huang, J.-S.; Biagioni, P.; Prangsma, J. C.; Hecht, B. Atomic-scale confinement of resonant optical fields. *Nano Lett.* **2012**, *12*, 5504–5509.
- (16) Ding, S.-Y.; Yi, J.; Li, J.-F.; Ren, B.; Wu, D.-Y.; Panneerselvam, R.; Tian, Z.-Q. Nanostructure-based plasmon-enhanced Raman spectroscopy for surface analysis of materials. *Nat. Rev. Mater.* **2016**, *1*, 16021.

- (17) Fernández-Domínguez, A. I.; Bozhevolnyi, S. I.; Mortensen, N. A. Plasmon-enhanced generation of nonclassical light. *ACS Photonics* **2018**, *5*, 3447–3451.
- (18) Yuan, L.; Bourgeois, B. B.; Carlin, C. C.; da Jornada, F. H.; Dionne, J. A. Sustainable chemistry with plasmonic photocatalysts. *Nanophotonics* **2023**, *12*, 2745–2762.
- (19) Wang, Y.; Abb, M.; Boden, S. A.; Aizpurua, J.; de Groot, C. H.; Muskens, O. L. Ultra-fast nonlinear control of progressively loaded, single plasmonic nanoantennas fabricated using helium ion milling. *Nano Lett.* **2013**, *13*, 5647–5653.
- (20) Hu, H. C.; Ji, F.; Xu, Y.; Yu, J. Q.; Liu, Q. P.; Chen, L.; Chen, Q.; Wen, P.; Lifshitz, Y.; Wang, Y.; Zhang, Q.; Lee, S.-T. Reversible and precise self-assembly of Janus metal-organosilica nanoparticles through a linker-free approach. *ACS Nano* **2016**, *10*, 7323–7330.
- (21) Manfrinato, V. R.; Stein, A.; Zhang, L.; Nam, C.-Y.; Yager, K. G.; Stach, E. A.; Black, C. T. Aberration-corrected electron beam lithography at the one nanometer length scale. *Nano Lett.* **2017**, *17*, 4562–4567.
- (22) Kim, I.; Mun, J.; Baek, K. M.; Kim, M.; Hao, C.; Qiu, C.-W.; Jung, Y. S.; Rho, J. Cascade domino lithography for extreme photon squeezing. *Mater. Today* **2020**, *39*, 89–97.
- (23) Romero, I.; Aizpurua, J.; Bryant, G. W.; García de Abajo, F. J. Plasmons in nearly touching metallic nanoparticles: singular response in the limit of touching dimers. *Opt. Express* **2006**, *14*, 9988–9999.
- (24) Zhu, W.; Esteban, R.; Borisov, A. G.; Baumberg, J. J.; Nordlander, P.; Lezec, H. J.; Aizpurua, J.; Crozier, K. B. Quantum mechanical effects in plasmonic structures with subnanometre gaps. *Nat. Commun.* **2016**, *7*, 11495.

- (25) Esteban, R.; Borisov, A. G.; Nordlander, P.; Aizpurua, J. Bridging quantum and classical plasmonics with a quantum-corrected model. *Nat. Commun.* **2012**, *3*, 825.
- (26) Liu, D.; Wu, T.; Zhang, Q.; Wang, X.; Guo, X.; Su, Y.; Zhu, Y.; Shao, M.; Chen, H.; Luo, Y.; Lei, D. Probing the in-plane near-field enhancement limit in a plasmonic particle-on-film nanocavity with surface-enhanced Raman spectroscopy of graphene. *ACS Nano* **2019**, *13*, 7644–7654.
- (27) Raza, S.; Wubs, M.; Bozhevolnyi, S. I.; Mortensen, N. A. Nonlocal study of ultimate plasmon hybridization. *Opt. Lett.* **2015**, *40*, 839–842.
- (28) Yang, B.; Chen, G.; Ghafoor, A.; Zhang, Y.; Zhang, Y.; Zhang, Y.; Luo, Y.; Yang, J.; Sandoghdar, V.; Aizpurua, J.; Dong, Z.; Hou, J. G. Sub-Nanometre Resolution in Single-Molecule Photoluminescence Imaging. *Nat. Photon.* **2020**, *14*, 693–699.
- (29) Lee, J.; Crampton, K. T.; Tallarida, N.; Apkarian, V. A. Visualizing vibrational normal modes of a single molecule with atomically confined light. *Nature* **2019**, *568*, 78–82.
- (30) Benz, F.; Schmidt, M. K.; Dreismann, A.; Chikkaraddy, R.; Zhang, Y.; Demetriadou, A.; Carnegie, C.; Ohadi, H.; De Nijs, B.; Esteban, R.; Aizpurua, J.; Baumberg, J. J. Single-molecule optomechanics in “picocavities”. *Science* **2016**, *354*, 726–729.
- (31) Li, W.; Zhou, Q.; Zhang, P.; Chen, X.-W. Bright optical eigenmode of 1 nm<sup>3</sup> mode volume. *Phys. Rev. Lett.* **2021**, *126*, 257401.
- (32) Wu, T.; Yan, W.; Lalanne, P. Bright Plasmons with Cubic Nanometer Mode Volumes through Mode Hybridization. *ACS Photonics* **2021**, *8*, 307–314.
- (33) Lu, Z.; Ji, J.; Ye, H.; Zhang, H.; Zhang, S.; Xu, H. Quantifying the Ultimate Limit of Plasmonic Near-field Enhancement. *Nat. Commun.* **2024**, *15*, 8803.

- (34) Mortensen, N. A. Mesoscopic electrodynamics at metal surfaces. *Nanophotonics* **2021**, *10*, 2563–2616.
- (35) Stamatopoulou, P. E.; Tserkezis, C. Finite-size and quantum effects in plasmonics: manifestations and theoretical modelling. *Opt. Mater. Express* **2022**, *12*, 1869–1893.
- (36) Kern, J.; Kullock, R.; Prangma, J.; Emmerling, M.; Kamp, M.; Hecht, B. Electrically driven optical antennas. *Nat. Photon.* **2015**, *9*, 582–586.
- (37) Bigourdan, F.; Hugonin, J.-P.; Marquier, F.; Sauvan, C.; Greffet, J.-J. Nanoantenna for electrical generation of surface plasmon polaritons. *Phys. Rev. Lett.* **2016**, *116*, 106803.
- (38) Li, W.; Zhou, Q.; Zhang, P.; Chen, X.-W. Direct electro plasmonic and optic modulation via a nanoscopic electron reservoir. *Phys. Rev. Lett.* **2022**, *128*, 217401.
- (39) Zurak, L.; Wolff, C.; Meier, J.; Kullock, R.; Mortensen, N. A.; Hecht, B.; Feichtner, T. Modulation of surface response in a single plasmonic nanoresonator. *Sci. Adv.* **2024**, *10*, eadn5227.
- (40) Marinica, D.; Kazansky, A.; Nordlander, P.; Aizpurua, J.; Borisov, A. G. Quantum Plasmonics: Nonlinear Effects in the Field Enhancement of a Plasmonic Nanoparticle Dimer. *Nano Lett.* **2012**, *12*, 1333–1339.
- (41) Prodan, E.; Radloff, C.; Halas, N. J.; Nordlander, P. A hybridization model for the plasmon response of complex nanostructures. *Science* **2003**, *302*, 419–422.
- (42) Zuloaga, J.; Prodan, E.; Nordlander, P. Quantum description of the plasmon resonances of a nanoparticle dimer. *Nano Lett.* **2009**, *9*, 887–891.
- (43) Ciracì, C.; Hill, R. T.; Mock, J. J.; Urzhumov, Y.; Fernández-Domínguez, A. I.; Maier, S. A.; Pendry, J. B.; Chilkoti, A.; Smith, D. R. Probing the ultimate limits of plasmonic enhancement. *Science* **2012**, *337*, 1072–1074.

- (44) Savage, K. J.; Hawkeye, M. M.; Esteban, R.; Borisov, A. G.; Aizpurua, J.; Baumberg, J. J. Revealing the quantum regime in tunnelling plasmonics. *Nature* **2012**, *491*, 574–577.
- (45) Scholl, J. A.; Koh, A. L.; Dionne, J. A. Quantum plasmon resonances of individual metallic nanoparticles. *Nature* **2012**, *483*, 421–427.
- (46) Scholl, J. A.; García-Etxarri, A.; Koh, A. L.; Dionne, J. A. Observation of quantum tunneling between two plasmonic nanoparticles. *Nano Lett.* **2013**, *13*, 564–569.
- (47) Khurgin, J.; Tsai, W.-Y.; Tsai, D. P.; Sun, G. Landau damping and limit to field confinement and enhancement in plasmonic dimers. *ACS Photonics* **2017**, *4*, 2871–2880.
- (48) Tserkezis, C.; Mortensen, N. A.; Wubs, M. How nonlocal damping reduces plasmon-enhanced fluorescence in ultranarrow gaps. *Phys. Rev. B* **2017**, *96*, 085413.
- (49) Yang, Y.; Zhu, D.; Yan, W.; Agarwal, A.; Zheng, M.; Joannopoulos, J. D.; Lalanne, P.; Christensen, T.; Berggren, K. K.; Soljačić, M. A general theoretical and experimental framework for nanoscale electromagnetism. *Nature* **2019**, *576*, 248–252.
- (50) Yan, W.; Wubs, M.; Mortensen, N. A. Projected Dipole Model for Quantum Plasmonics. *Phys. Rev. Lett.* **2015**, *115*, 137403.
- (51) Christensen, T.; Yan, W.; Jauho, A.-P.; Soljačić, M.; Mortensen, N. A. Quantum Corrections in Nanoplasmonics: Shape, Scale, and Material. *Phys. Rev. Lett.* **2017**, *118*, 157402.
- (52) Raza, S.; Toscano, G.; Jauho, A.-P.; Wubs, M.; Mortensen, N. A. Unusual resonances in nanoplasmonic structures due to nonlocal response. *Phys. Rev. B* **2011**, *84*, 121412(R).
- (53) Toscano, G.; Straubel, J.; Kwiatkowski, A.; Rockstuhl, C.; Evers, F.; Xu, H.;

- Mortensen, N. A.; Wubs, M. Resonance shifts and spill-out effects in self-consistent hydrodynamic nanoplasmonics. *Nat. Commun.* **2015**, *6*, 7132.
- (54) Yan, W. Hydrodynamic theory for quantum plasmonics: Linear-response dynamics of the inhomogeneous electron gas. *Phys. Rev. B* **2015**, *91*, 115416.
- (55) Ciraci, C.; Della Sala, F. Quantum hydrodynamic theory for plasmonics: Impact of the electron density tail. *Phys. Rev. B* **2016**, *93*, 205405.
- (56) Ciraci, C. Current-dependent potential for nonlocal absorption in quantum hydrodynamic theory. *Phys. Rev. B* **2017**, *95*, 245434.
- (57) Baghramyani, H. M.; Della Sala, F.; Ciraci, C. Laplacian-level quantum hydrodynamic theory for plasmonics. *Phys. Rev. X* **2021**, *11*, 011049.
- (58) Lalanne, P.; Yan, W.; Vynck, K.; Sauvan, C.; Hugonin, J.-P. Light interaction with photonic and plasmonic resonances. *Laser Photon. Rev.* **2018**, *12*, 1700113.
- (59) Yan, W.; Faggiani, R.; Lalanne, P. Rigorous modal analysis of plasmonic nanoresonators. *Phys. Rev. B* **2018**, *97*, 205422.
- (60) Zhou, Q.; Zhang, P.; Chen, X.-W. Quasinormal mode theory for nanoscale electromagnetism informed by quantum surface response. *Phys. Rev. B* **2022**, *105*, 125419.
- (61) Zhou, Q.; Zhang, P.; Chen, X.-W. General framework of canonical quasinormal mode analysis for extreme nano-optics. *Phys. Rev. Lett.* **2021**, *127*, 267401.
- (62) Kamandar Dezfouli, M.; Tserkezis, C.; Mortensen, N. A.; Hughes, S. Nonlocal quasinormal modes for arbitrarily shaped three-dimensional plasmonic resonators. *Optica* **2017**, *4*, 1503–1509.
- (63) Binkowski, F.; Zschiedrich, L.; Hammerschmidt, M.; Burger, S. Modal analysis for nanoplasmonics with nonlocal material properties. *Phys. Rev. B* **2019**, *100*, 155406.



- (64) Raza, S.; Bozhevolnyi, S. I.; Wubs, M.; Mortensen, N. A. Nonlocal optical response in metallic nanostructures. *J. Phys.: Cond. Matter* **2015**, *27*, 183204.
- (65) Halevi, P. Hydrodynamic model for the degenerate free-electron gas: generalization to arbitrary frequencies. *Phys. Rev. B* **1995**, *51*, 7497–7499.
- (66) Wegner, G.; Huynh, D.-N.; Mortensen, N. A.; Intravaia, F.; Busch, K. Halevi’s extension of the Euler-Drude model for plasmonic systems. *Phys. Rev. B* **2023**, *107*, 115425.
- (67) Yoon, J. H.; Selbach, F.; Schumacher, L.; Jose, J.; Schlücker, S. Surface plasmon coupling in dimers of gold nanoparticles: experiment and theory for ideal (spherical) and nonideal (faceted) building blocks. *ACS Photonics* **2019**, *6*, 642–648.
- (68) Tserkezis, C.; Taylor, R. W.; Beitner, J.; Esteban, R.; Baumberg, J. J.; Aizpurua, J. Optical response of metallic nanoparticle heteroaggregates with subnanometric gaps. *Part. Part. Syst. Charact.* **2014**, *31*, 152–160.
- (69) Tserkezis, C.; Herrmann, L. O.; Valev, V. K.; Baumberg, J. J.; Aizpurua, J. Optical response of threaded chain plasmons: from capacitive chains to continuous nanorods. *Opt. Express* **2014**, *22*, 23851–23860.
- (70) Zhang, Q.; Cai, X.; Yu, X.; Carregal-Romero, S.; Parak, W. J.; Sachan, R.; Cai, Y.; Wang, N.; Zhu, Y.; Lei, D. Y. Electron Energy-Loss Spectroscopy of Spatial Nonlocality and Quantum Tunneling Effects in the Bright and Dark Plasmon Modes of Gold Nanosphere Dimers. *Adv. Quantum Technol.* **2018**, *1*, 1800016.
- (71) Pérez-González, O.; Zabala, N.; Borisov, A. G.; Halas, N. J.; Nordlander, P.; Aizpurua, J. Optical spectroscopy of conductive junctions in plasmonic cavities. *Nano Lett.* **2010**, *10*, 3090–3095.